BILINGUAL PUBLISHING CO.
Pioneer of Global Academics Since 1984

Advances in Geological and Geotechnical Engineering Research
https://ojs.bilpublishing.com/index.php/agger

ARTICLE

Integrated Hydrogeochemical Analysis of Stream Water in Parts of Proterozoic Shillong Basin Meghalaya, India

A.P. Dhurandhar*

Katol Road, Nagpur, 440013, India

ARTICLE INFO

Article history
Received: 08 March 2022
Revised: 11 April 2022
Accepted: 18 April 2022
Published Online: 25 April 2022

Keywords:
Hydrogeochemistry
Water quality
Subsurface relations
Shillong basin

ABSTRACT

Hydrogeochemical surveys were conducted in parts of the Proterozoic Shillong basin in Meghalaya to locate the unconformity-related uranium deposits, related alteration patterns, and the influence of the rock formations on the groundwater solute chemistry. Shillong Basin comprises Proterozoic metasediments and felsic volcanics of Tyrsad Formation, undeformed arenaceous Barapani Formation with intrusive granites, and metabasic sills and dykes. The groundwater quality is determined for drinking, and domestic-agro-industrial utilities using hydrogeochemical tools and physicochemical parameters. The water is acidic to slightly alkaline and has an oxidizing redox environment, Electrical Conductivity (EC), Total Dissolve Solids (TDS), and major ions fell below the World Health Organization (WHO) and Indian Standards Institute (ISI) acceptable limits except for Zn, Fe, and SiO_2 showing higher concentrations. The sequences of abundance of major cations and trace elements are $Fe>Zn>SiO_2>Ca^{2+}>Na^{+}>Mg^{2+}>K^{+}>U$ and anions as $HCO_3>Cl^{-}>SO_4^{2-}$. Groundwater character was assessed by ion exchange, simple dissolution, and unusual dissolution mechanisms. The area has dominant $CaHCO_3$, $NaHCO_3$, and restricted $CaMgHCO_3$ type water. Plagioclase dissolution and high SiO_2 and cation exchange of Ca for Na were identified. The groundwater indices of Sodium Percent, Kelley's Index, Sodium Adsorption Ratio, Magnesium Ratio, Electrical Conductivity, TDS, USSL, and Wilcox index were found suitable for agro-industrial uses. Permeability Index is found to be suitable in most areas and the Corrosivity Ratio shows the areas of galvanized pipes and PVC pipes to be used for water supply. AHC analysis shows three distinct groups of water types, as well as the factor analysis, also shows the three prominent factors of water types defining the dimensionality of water types. Magnesium metasomatic alteration zones and Zn anomalous zones are delineated.

*Corresponding Author:
A.P. Dhurandhar,
Katol Road, Nagpur, 440013, India;
Email: apdhurandhar@gmail.com

DOI: https://doi.org/10.30564/agger.v4i2.4498

1. Introduction

The objective of the hydrogeochemical survey in the present study is to explore the possibilities of Proterozoic unconformity-related uranium deposits in Shillong Basin Meghalaya. Traditional mineral prospecting methods present an obstacle when applied to areas with transported cover and very high gradient, especially where the coverage is larger than a few meters thick, as in the Shillong basin. Groundwater, a geochemical sample that travels through the subsurface, is easy to collect and can be evaluated with high sensitivity and precision. It presents a chemical fingerprint of mineralization due to varying Eh-pH conditions, alteration, clay adsorption, and clays and hydrous metal oxides such as iron and manganese which can directly change the uranyl ions' mobility and dispersal [1-3]. Groundwaters that drain through various rock types like igneous, metamorphics, and sedimentary (felsic, alkali, basics) can also change the uranium concentration in groundwater and may give rise to pseudo uranium anomalies. True uranium anomalies can be overlooked if the effect of local surface or rainwater dilution is not recognized. A regional ground-water study can indicate where target formations occur within the economic range of the surface. Anthropogenic activities/ requirements such as mining activities and related pollution, and drinking water scarcity are major concerns and hence necessitate water quality monitoring [4]. The Shillong plateau is a high rainfall area but the nearby cities, towns, and villages mainly depend upon the rainwater, spring, and river water for drinking and irrigation purposes. Due to stricter legislation on soil and groundwater contamination and increasing population and demand in food production, Hydrogeochemistry is complex and needs to be evaluated in the context of bedrock geology, regolith development, regional groundwater flow, and anthropogenic disturbances before assessing the effects of mineralization on the chemistry. Major ion composition of groundwater is important as it can identify water types, mixing, evaporation, water-rock interaction, and recharge of the particular groundwater system. However, some studies have also suggested that the major ion composition of groundwater can provide direct vectors to mineralization, in particular owing to the generally larger target provided by alteration halos around mineralization relative to the size of primary ore mineralization [4-6]. Hydrogeochemistry and water management in agriculture are aiming for better tools to estimate risk assessment. Water quality assessment is a major value-added by-product of such investigations. Such studies have never been carried out in parts of the Shillong basin.

2. Geology and Structures

The surveyed area exposes Proterozoic lithologies consisting of metasediments and volcanics of Tyrsad Formation, undeformed arenaceous Barapani Formation with intrusive granites, and metabasic sills and dykes (Figure 1). The metasedimentary rocks of the Shillong group can be divided into two broad lithofacies [7], the older argillaceous and the younger arenaceous. Tyrsad Formation is a metasedimentary sequence consisting of phyllites to schistose units such as carbon phyllite/ graphitic schist, phyllite/slate, chlorite schist, sericite schist, chlorite-sericite schist, mica schist, and quartzite (Table 1). In the south of the NE-SW trending Umiam river chloritic phyllite and chlorite schist are the dominant litho units while in the north of the Umiam river sericite schist and chlorite-sericite schist are the dominant litho units. Along the Nongpinom-Mawklot, Umlyngka tract carbon phyllite is exposed along the small river (rivulet) sections just below the conglomerate horizon, which invariably contains pyrites. Alteration features like chloritisation are intense in Tyrsad Formation throughout the area and sericitization in the northern part along the Mawpun-Nongbsap tract. The volcanic component of the Tyrsad Formation consists of rhyolite, intermediate volcanics, and quartz porphyry. Sheared rhyolites are dominating the northern margin of the area. The unconformity contact between Tyrsad and Barapani Formation is erosional and marked by the development of a thick conglomerate bed at the base of the Barapani Formation. The conglomerate is polymictic, clast supported, and consists of pebbles of quartzite, quartz, and volcanic components derived from the underlying Tyrsad Formation. The pebbles are stretched and sheared and the matrix is schistose and foliated. Unconformity contact in the surveyed area is traced along the north of Laitjem to the southeast of Lummwablei village. The Barapani Formation is an arenaceous sequence that rests unconformably above the metasediments and volcanics of the Tyrsad Formation. It starts with a basal sheared conglomerate followed by pebbly arenite, coarse cream-colored arenite, and whitish friable arenite showing a fining upward sequence north of Mawtawar village. The arenites are cream to grey colored, medium to coarse-grained with argillaceous material as the matrix. Barapani formation occupies a large part of the surveyed area. The regional strike of the Shillong group of rocks is NE-SW with alternate rolling dips and steep subvertical zones [7,8]. A shear zone extending from Tyrsad to Barapani (Figure 1b, 1c) was described based on slickensides [9-11]. The

regional sigmoidal pattern of the intraformational conglomerate broadly correlates with the Tyrsad-Barapani Shear Zone (TBSZ) of sinistral nature. Barapani Formation at places shows intense ferruginisation and limonitisation (Umlyngka - Umiam river road section) along the ENE-WSW, and NNE-SSW trending fracture. Ferruginisation is intense at the intersection of these two fractures. This ferruginisation and limonitisation processes indicate extensive oxidation in Barapani arenite. Argillisation is also observed in the axial portion of the folded Barapani arenite along the Nongumlong-Umiam, and Lummawsiang-Umsaw road section. Sedimentary structures such as current bedding, cross-bedding, and graded bedding are well preserved in the Barapani Formation. In the surveyed area Neoproterozoic to early Paleozoic granites such as Mylliem granite (607±13 Ma), and Kyrdem granite (479±26 Ma) intrude the rocks of the Barapani Formation with sharp intrusive contact [12,13]. The amphibolites and metadolerites intrudes both Barapani and Tyrsad Formations as sills and dykes, showing NE-SW to ENE-WSW trend. Metadoleritic dykes of both fresh and sheared nature are observed in this area (Um Ban rivulet, Nongumlong-Umiam river road section, N of Laitjem-Mawkrih-Nongpinom).

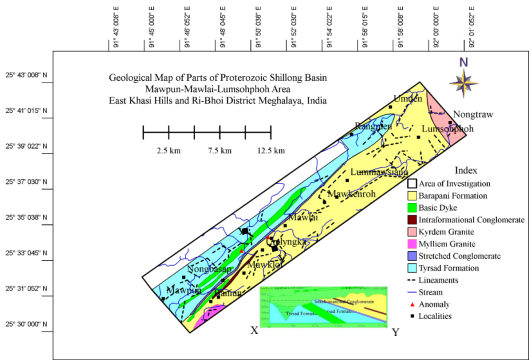

1a.

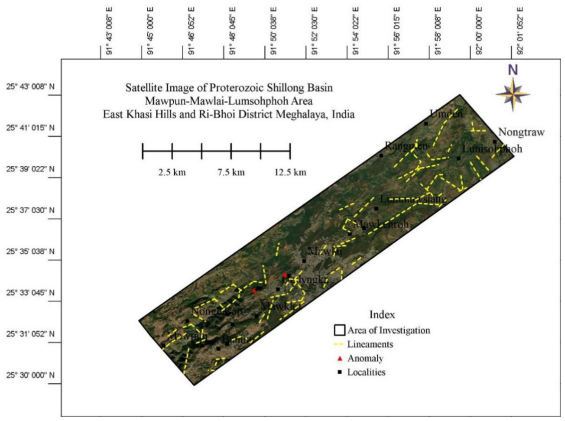

1b.

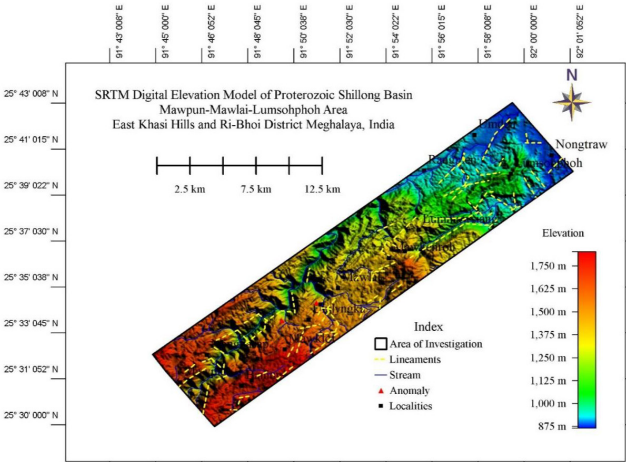

1c.

Figure 1. 1a: Geological map of the study area. 1b: Satellite Image of the study. 1c: Shuttle Radar Topographic Mission (SRTM) data of the study area.

Table 1. Lithostratigraphic succession of the study area.

Era	Formation	Lithology
Late Proterozoic Early Palaeozoic	Kyrdem Granite (479±26Ma) Mylliem Granite (607±13Ma)	Coarse, porphyritic grey, and pink granites Zircon ages of 430-480 and 500Ma
Intrusive contct		
	Metabasic intrusives	Sheared meta-doleritic sills and dykes
Intrusive contact		
Meso-Proterozoic	Barapani Formation	Cream colored, current and cross-bedded, Quartz arenite (> 560-Ma detrital zircons) with shaly intercalations, Pebbly and gritty arenite(±pyrites),
Sheared, stretched, clast supported Polymictic conglomerate		
Palaeo-Proterozoic	Tyrsad Formation	Rhyolite, intermediate volcanics Carbon phyllite/Graphitic schist (pyrites) Phyllite/Slate, Chlorite schist, Sericite schist Chlorite sericite schist, mica schist Quartzite (>1100 Ma detrital zircon)
Unconformity		
Basement gneissic complex not exposed (1100 to 1650 Ma based on Zircon dates)		

N.B. Kyrdem and Mylliem Granite Rb-Sr dates after [10,11], and Zircon ages are after [16].

Structural Setting

The Proterozoic litho units of the surveyed area show a regional foliation of NE-SW to ENE-WSW with 40° to subvertical dips SE-SSE in Tyrsad Formation and 10° to 25° SE, SSE in Barapani Formation. The structural history of the rocks of Shillong Group in the study area depicts four phases of deformation; viz: a sub-horizontal simple shear in NW-SE direction acting on horizontal beds gave rise to recumbent, isoclinal F_1 fold with NE-SW axial trend. The F_2 folds have developed when simple shear gave way to pure shear with NW-SE compression so that upright folds with NNE axial trend resulted, rotating the axial planes of F_1 folds coaxially with the development of crenulation cleavage [14,15]. The F_3 folds developed locally due to maximum compression in vertical to subvertical thinly layered rocks so that there is continuity in the first three stages of deformation which is revealed by these three sets of coaxial folds. The F_4 folds are open warps with different axial trends E-W, N-S, NW-SE, developed entirely in a different pattern by horizontal compression in a NE-SW direction in the last stage of deformational episode equally supported by the lineament rose diagram (Figure 2). The lithostructural mapping was also carried out using satellite images namely Landsat 8 OLI and Sentinel 2 data in conjunction with the SRTM digital terrain models (Figure 1b and 1c). The F_4 structures, therefore, furnish evidence of longitudinal shortening in the final stage of deformation Umlyngka-Umiam river road section. NE-SW trending Tyrsad-Barapani shear zone is characterized by:

i. Drastic reduction in grain size of the country rocks.

ii. Intense silicification.

iii. Development of hydrous phases of mineral and incipient gossans.

iv. The regional sigmoidal pattern of the intraformational conglomerate broadly correlates with the Tyrsad-Barapani Shear Zone (TBSZ) of sinistral nature [14]. In the surveyed area this shear zone is manifested by the presence of sheared conglomerate, slickensides / striated limbs of F_1 folds in chloritic phyllite, altered basic rocks, and NE - SW trending ridges [15,16].

In Barapani Formation, folds are of the open type with NE-SW axial trend. The NNE-SSW & ENE-WSW trending fractures are common. Tyrsad Formation has been affected by three distinct phases of deformation while the Barapani Formation has been subjected to only the last two phases of deformation thus suggesting younger age. Intense deformation led to recrystallization corresponding to a higher almandine-amphibolite grade of metamorphism [15,16]. The second deformation phase is associated with retrograde greenschist facies of metamorphism, which is indicated by the growth of axial planer biotite and chlorite and chloritization of garnet. Integrated structural and geochronological investigations reveal that the Shillong plateau has been affected by four phases of magmatism at ca. 1600 Ma, ca. 1100 Ma, ca. 500 Ma, and ca. 105 Ma-95 Ma, and four episodes of deformation at 1100 Ma, 500 Ma, 100 Ma, and 20 Ma-0 Ma have been documented [17]. This analysis suggests that the intrusive granites and Augen gneisses contain inherited zircon dating 1600 Ma-1100 Ma and the second phase of granites contains 520 Ma-430 Ma zircon which means the Shillong group of rocks i.e., sandstone and shale upper part contains > 560-Ma detrital zircons, and the lower part contains >1100 Ma detrital zircon. The sequence (Shillong group) is intruded by 520 Ma-480 Ma granitoids and isoclinal foldings and concomitant deformations in the Shillong group have occurred between 520 Ma to 500 Ma (Age of the two deformations due to granitic intrusions).

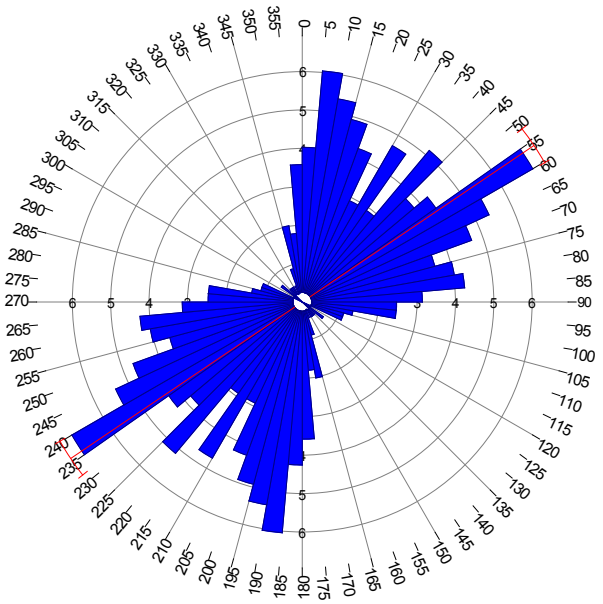

N= 447

Vector mean =55.98°N

Figure 2. Lineament Rose diagram for Shillong Basin

3. Geomorphology and Hydrogeology

Geomorphologically the area shows a moderately dissected hill (Northern part) and dissected Plateau in the southern part. The dissection of these areas is mainly due to lineament-controlled drainage systems. The dominant trend of lineaments in the Shillong basin is NNE-SSW. In the central part of the Shillong basin, the crystalline and metasedimentaries are peneplained to gently sloping surfaces and are grouped in dissected

Plateaux. The dissection in the central part still preserves the old plateaux characters. Lineament-controlled drainage patterns with patches of sub-dendritic drainage characterize the area. In NE-SW trending fault zones, escarpments are common. Lineaments are either straight or curvilinear in NNE-SSW directions [18].

The temperature ranges from 1.7 °C to 24 °C, and the climate ranges from temperate humid to subtropical humid. The area receives very high rainfall, the rainy season is from April to October, though none of the months is completely dry. December's driest month, with 19 mm (0.7 inches) of rainfall. Most of the precipitation here falls in July, averaging 714 mm (28.1 inches). The months with the greatest temperatures are also those with the wettest weather, making the environment humid [19]. The northern areas of Shillong are also distinguished by the existence of a variety of rivers, including the Umtrew, Umiam, and Umkhen. The Brahmaputra River is fed by rivers in the northern section of the area. The Quartzite deposit of the Proterozoic Shillong Group lacks primary porosity. Groundwater circulation and occurrence are influenced by physiography, weathering zones, and linked zones of weakness or secondary porosity, such as joints and faults. Groundwater exists in two states: unconfined in weathered residuum and semi-confined in secondary porosity such as cracks and fissures. The depth to water level ranges from 2 m to 26 m below ground level. The majority of the area is occupied by quartzite and granite rocks having a groundwater potential of 5 m^3/hr-15 m^3/hr [20,21]. In most of the areas in valley sections, the topography cuts the water table and forms a natural spring.

4. Materials and Methodology

A total of 108 water samples were collected from the 1st and 2nd order streams draining in the survey area of 175 km^2 with a sampling density of 1:1.62 km^2. The stream and spring water sampling was done during the post-monsoon period (November-January) when stream flows remain constant. The sampling was suspended during the storm runoff periods after the heavy rains in the area. The water table is dissected by topography giving rise to several springs in the survey area. The samples were collected from such springs after a few tens of meters of surface flow. The data collection methods are similar to standard hydrogeochemical sampling methods described by Brown and Woods et al. [22,23]. However, appropriate quality assurance (QA) and quality control (QC) measures were performed during sample collection and analysis. Data screening and duplicate removal were carried out before processing. The Total Dissolved Solids (TDS), EC, and pH of water samples were measured in the field immediately after the sampling. Ca and Mg were determined by standard Ethylene Diamine Tetra Acetic acid (ETDA). Na and K were measured by a Flame photometer, Cl by Volhard's titration and HCO_3 by acid-base titration, and SO_4 by Systronic turbidity meter. SiO_2 was measured by a UV spectrophotometer. Trace elements Zn and Fe were measured by Atomic Absorption Spectrophotometer (AAS) and U by UA3 Laser Fluorometer. The entire database has 14 variables, including physicochemical parameters (TDS, conductivity, pH), cations (Na, K, Ca, Mg,), anions (Cl, CO_3, HCO_3, SO_4), and trace elements (Fe, Zn, U) in Table 2.

Table 2. Hydrogeochemical data summary statistics

Parameters	Minimum	Maximum	Median	Arithmetic Mean	Standard Deviation	WHO Limits 2011 [29]	ISI Limits 1974 [52]
Na	0.05	12.10	2.25	2.75	2.48	200	
K	0.05	5.60	0.65	0.92	1.01	10	
Ca	0.05	16.00	2.20	3.74	3.63	100-200	75-200
Mg	0.10	13.00	1	1.25	1.62	50	30-100
Cl	3.00	36.00	6	7.52	5.14	250	600
HCO_3	3.00	393.40	21.00	39.37	61.75	200	
Fe	5.00	625.00	47.50	107.11	138.53	0.1	0.3
TDS	2.00	180.00	35	42	31.07		
pH	3.40	8.40	6.90	6.79	0.67	6.5-8.5	6-9
COND. µS/cm	5.00	284.00	30.50	42.51	38.88	1.6	0.8-2.4
ALK.	5.00	644.80	35	64.78	100.99		600*
TH	0.50	71	9.40	13.60	11.59	500	300
SiO_2	0.90	40.43	8.98	11.12	8.75		

Table 2 continued

Parameters	Minimum	Maximum	Median	Arithmetic Mean	Standard Deviation	WHO Limits 2011 [29]	ISI Limits 1974 [52]
Zn ppb	0.50	9039	3.00	98.80	876.90	5	5
SO_4	3	3	3	3	0	200-400	150-400
NMg	0.05	0.83	0.22	0.25	0.15		
pE	12.38	17.38	13.88	13.98	0.67		
Eh (V)	0.73	1.03	0.82	0.83	0.04		
% Na	2.19	69.63	34.94	34.01	16.19		
SAR	0.07	8.51	1.70	2.07	1.63		
PS	0.09	1.02	0.20	0.23	0.15		
PI	28.60	1493.33	89.41	130.09	163.06		
MR	5.96	97.06	34.81	37.21	16.21		
CR	0.02	16.90	0.55	0.76	1.63		
CAI-I	–3.53	0.81	–0.37	–0.57	0.77		
KI	0.02	2.13	0.42	0.52	0.41		

Note: 1. The number of samples n = 108, all units in mg/L, except those mentioned *Central Pollution Control Board India. 2. Uranium except for three samples, all are below detection limits, 0.7 ppb UM/2, NONG/5, and 0.8 ppb MYL/4. Whereas all other trace elements values are below detection limits for the entire investigated area.

The U content is <0.5 ppb in all the samples except three samples which show 0.7 ppb (UM/2, NONG/5) and 0.8 ppb (MYL/4), these sample locations are shown in Figure 3a and 3b as red hollow diamonds. All other trace elements analyzed are below detection limits for the entire area investigated. Water chemistry data are frequently hampered by censored values, in that the concentration of certain elements is reported only as less than (<) or greater than (>). These values represent the lower and upper detection limits of the instrument. These censored values should be replaced with unqualified values since they are unsuitable for imaging and statistical analysis [24,25]. The strategy followed for the present study for the replacement of less-than values by 0.55 times the lower detection limit and greater-than values by 1.7 times the upper detection limit, given by [26]. This method is followed to fill the < the detection limit values in some uranium and SO_4. Spatial distribution images were generated using Golden Surfer with standard gridding and interpolation methods such as I^2DW. SRTM digital elevation model was generated using Global mapper. Landsat 8 OLI and Sentinel 2 data were interpreted for lithostructural mapping. Statistical analysis is done on the XLSTAT plugin for excel. The uranium along with the SO_4 image not generated as well as not considered for statistical analysis since it shows almost constant values for the entire area of investigation. Geological, radiometric and hydrogeochemical multi-elemental litho- and pedo-geochemical investigations were conducted for the investigated area.

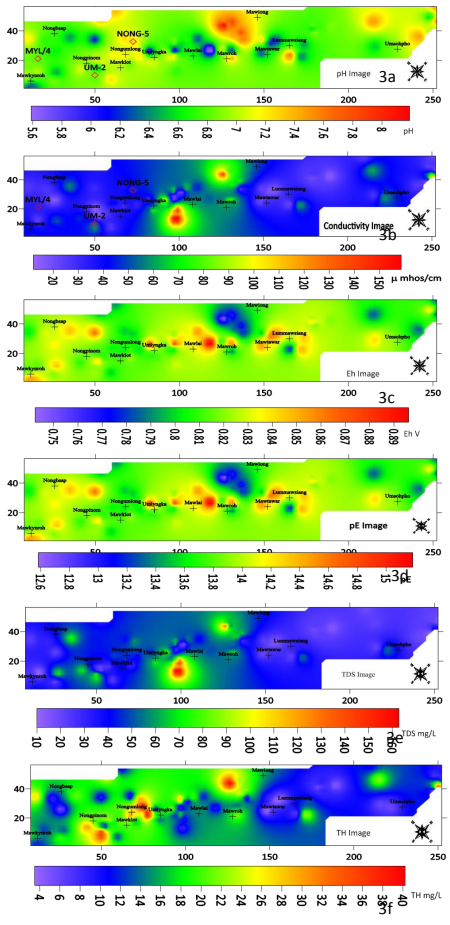

Figure 3. Images of Physicochemical parameters. 3a: pH Image, 3b: Conductivity Image, 3c: Eh image, 3d: pE image, 3e: TDS image, 3f: Total Hardness image

5. Results and Discussions

5.1 Physicochemical Parameters pH, Electrical Conductivity, Eh, pE and TDS

pH is a term used universally to express the intensity of the acid or alkaline condition of a solution. It is observed that the pH values of the water samples ranged from 3.4 to 8.4 with a mean value of 6.79 in the study area (Figure 3a). Acidic values observed may be due to the influx of rainwater of low alkalinity. The recommended values for irrigation water are from 6.5 to 8.4, and the permissible limits as per world health organization [27] are between 6.5 to 8.5.

Electrical conductivity ranges from 5 to 284 µ mhos/cm with an average of 42.51 µ mhos/cm (Figure 3b) the highest values are seen in the vicinity of SW of Mawlai and Mawiong. According to world health organization [27] guidelines; the permissible limit of EC is 1400 µ mhos/cm (Table 3). The oxidation-reduction potential (Eh = 0.059 pE) varies in the investigated area from 0.73 V to 1.03 V with an average of 0.83V indicating the water has strong oxidising environment Figure 3c, [27,30,31]. pE is calculated in the field by measuring pH (pe = 20.775-pH). pE is varying from 12.38 to 17.38 with an average of 13.88 (Figure 3d). This is also unitless as the pH of water. The uranium content measured 0.7 ppb (n=2) to 0.8 ppb (n=1) at localities are shown as red triangles in Figure 3a and 3b rest of the samples measured below detection limits of 0.5 ppb. The low U content in the water is caused by the lesser residence time available for water in rocks due to the higher gradient of terrain and high rainfall. This phenomenon is also reflected by low conductivity and low TDS 2-180 mg/L with an average of 42 mg/L (Figure 3e).

5.1.1 Total Dissolved Solids

TDS varies from 2 mg/L to 180 mg/L with an average of 43 mg/L and falls under the freshwater category (Table 3). The highest values are seen around SE of Mawlai and NE of Umlingka villages (Figure 3e).

Table 3. Classification of stream water quality based on suitability of water for drinking and irrigation and supply purposes.

Parameter	Range	Class	Number / %
Conductivity	<250	Excellent	107/99.1%
	250-750	Good	1/0.9%
	750-2000	Permissible	Nil
	2000-3000	Doubtful	Nil
	>3000	Unsuitable	Nil
TDS	0 -500	Desirable for Drinking	108/100%
	0 -1000	Freshwater Permissible for drinking	108/100%
	Up to 3000	Permissible for Drinking	Nil
	>3000	Unfit for drinking water	Nil
	1000-10000	Brackish Water	Nil
	10,000-100,000	Saline Water	Nil
	>100,000	Brine	Nil
Na%	<20	Excellent	27/25%
	20-40	Good	40/37.04%
	40-60	Permissible	34/31.48%
	60-80	Doubtful	7/6.48%
	>80	Unsuitable	Nil
MR	<50	Suitable	88/81.48%
	>50	Unsuitable	20/18.52%
TH	<75	Soft	108/100%
	75-150	Moderate	Nil
	150-300	Hard	Nil
	>300	Very hard	Nil

Table 3 continued

Parameter	Range	Class	Number / %
SAR	<20	Excellent	108/100%
	20-40	Good	Nil
	40-60	Permissible	Nil
	60-80	Doubtful	Nil
	>80	Unsuitable	Nil
KI	<1	Suitable	90/83.33%
	>1	Unsuitable	17/15.74
CR	<1	Galvanised Pipes to be used	89/82.41
	>1	Polyvinyl pipes to be used.	19/17.59%

5.1.2 Total Hardness (TH)

The TH of water is calculated as under:

$$HT = 2.5Ca + 1.5Mg \quad (1)$$

Total hardness varies from 0.50 to 71 with an average of 13.6 in Table 3 and Figure 3f. Temporary hardness is mainly due to calcium and magnesium ions and iron in the water that gets removed during heating. Permanent hardness is due to chlorides sulfates and nitrates of Ca^{2+} and Mg^{2+} ions that get removed by ion-exchange processes. The hardness of water limits its use for industrial purposes. For drinking water, the degree of hardness has been classified in terms of its equivalent concentration of $CaCO_3$. Table 4 shows that all the water samples of the study area belong to the soft category. In some studies, a significant correlation was observed between hardness and heart diseases, in contrast, several epidemiological studies suggest that water hardness protects against diseases [28].

5.2 Major Ions

5.2.1 Sodium (Na)

The Na^+ concentrations are varying from 0.05 mg/L to 12.1 mg/L with an average of 2.75 mg/L (Table 3), high zone is seen near the southwest of Mawlai and northwest of Umlygka village (Figure 4a). The major factors affecting Na distribution are similar to those of chloride and, to a lesser extent, SO_4^{2-}.

5.2.2 Potassium (K)

Generally, low potassium concentrations are observed in the entire survey area. The K values vary from 0.05 mg/L to 5.6 mg/L with an average of 0.92 mg/L, high zone is seen near the southwest of Mawlai and northwest of Umlygka village. Other areas of high K are observed over the granitic areas of Kyrdem and Mylliem near Umsophoh and Mawkynroh respectively (Figure 4b).

5.2.3 Calcium (Ca)

In general, Ca shows low concentration all over the study area. The values vary from 0.05 mg/L to 16 mg/L with an average of 3.74 mg/L (Figure 4c). Few high concentrations of Ca are observed near Nongpinom, Nongumlong and Mawlai, and Mawiong areas across the unconformity also from Barapani to Tyrsad formation.

5.2.4 Magnesium (Mg)

The dissolved Mg shows very good correlations with Ca in general, but in the present case, Mg values are very low in the study area ranging from 0.1 mg/L to 13 mg/L with an average of 1.62 mg/L (Table 3). The high Mg values are observed around Mawiong and in between Umlyngka and Nongumlong (Figure 4d).

5.2.5 Chloride (Cl)

In the present studied area, it varies from 3 mg/L to 36 mg/L with an average of 7.52 mg/L (Table 3). The spatial distribution is shown in (Figure 4e). The highest values are seen in between the Mawlai and Umlingka areas (Figure 4e). The principal effects on the chloride distribution are attributed to rainfall, lithology, and land-use patterns. Chloride in surface and groundwater is from both natural and anthropogenic sources, such as run-off containing road de-icing salts, inorganic fertilizers, landfill leachates, septic tank effluents, animal feeds, industrial effluents, irrigation drainage, and seawater intrusion in the coastal area. In natural waters, chlorides can be considered ubiquitous. Because chlorides are more of an aesthetic than a health concern (although high concentrations can be harmful to those with heart or kidney ailments), Chloride concentration in drinking water may be particularly important to persons on low salt

Table 4. Pearson's correlation of various parameters

	Na	K	Ca	Mg	Cl	HCO_3	Fe	TDS	pH	COND.	ALK.	TH	SiO_2	Zn	NMg
Na	1														
K	**0.76**	1													
Ca	**0.67**	**0.62**	1												
Mg	0.15	0.01	**0.62**	1											
Cl	**0.64**	**0.67**	**0.49**	0.02	1										
HCO_3	0.07	0.22	0.29	0.29	–0.11	1									
Fe	–0.02	0.18	–0.07	–0.07	–0.08	0.50	1								
TDS	**0.74**	**0.65**	**0.81**	**0.46**	**0.69**	0.00	–0.16	1							
pH	–0.28	–0.10	0.31	0.38	0.14	0.18	–0.05	0.09	1						
COND.	**0.81**	**0.73**	**0.92**	**0.54**	**0.62**	0.29	–0.03	**0.93**	0.09	1					
ALK.	0.07	0.21	0.28	0.29	–0.12	**1.00**	**0.50**	–0.01	0.18	0.28	1				
TH	0.37	0.21	**0.73**	**0.73**	0.04	**0.48**	0.12	0.32	0.33	**0.56**	**0.48**	1			
SiO_2	0.21	0.12	**0.65**	**0.66**	–0.19	0.39	–0.01	0.27	0.29	**0.47**	0.39	**0.81**	1		
Zn	–0.09	0.03	–0.12	–0.04	–0.04	**0.46**	**0.50**	0.04	–0.05	0.05	**0.47**	–0.09	–0.08	1	
NMg	**–0.62**	–0.42	–0.32	**0.29**	–0.33	**0.22**	0.08	–0.34	**0.33**	–0.35	**0.23**	–0.04	–0.04	**0.22**	1

NB: Bold positive correlations and red strong negative correlation

diets. The maximum contaminant level for public water supplies is 250 mg/L [29].

5.2.6 Bicarbonate (HCO3)

The levels of HCO_3 in samples from the study area are between 3 mg/L to 393.4 mg/L with an average of 39.37 mg/L. Results showed that only 1.8% of the groundwater samples had higher levels of HCO_3, exceeding the permissible limit. The high HCO_3 levels are observed in Umsohpho and SW of Mowiang Areas (Figure 4f). Bicarbonate concentration is a reliable measure of the extent of acid neutralization that has taken place in natural waters [30]. Bicarbonate anions are often dominant in natural stream waters and have a major influence on the solubility of several cations with which they form stable complexes. The higher proportions of bicarbonate with other anions indicate weathering of primary silicate minerals dominated by alkaline earth [31]. Other anions such as chloride and sulfate may be present in modest amounts in water with high bicarbonate levels. Bicarbonate raises the pH of water, and high bicarbonate levels may be linked to a high pH.

5.2.7 Alkalinity

Alkalinity varies from 5 to 644.8 with an average of 64.78 (Table 3, Figure 4g). Low alkaline values were observed due to the leaching of dissolved constituents into the water and the absence of calcareous rocks in the area. The $CaCO_3$ is not a health hazard [31,32]. Carbonate alkalinity makes up the majority of total alkalinity in the natural environment. Alkalinity can also be influenced by other natural elements. The dissolved carbon dioxide species, bicarbonate, and carbonate, provide alkalinity in practically all natural fluids. Borate, hydroxide, phosphate, silicate, nitrate, dissolved ammonia, conjugate bases of various organic acids, and sulfide are some of the most prominent noncarbonate sources of alkalinity. Alkalinity is vital because it buffers pH fluctuations that naturally occur during photosynthetic cycles, water exchanges, and other processes.

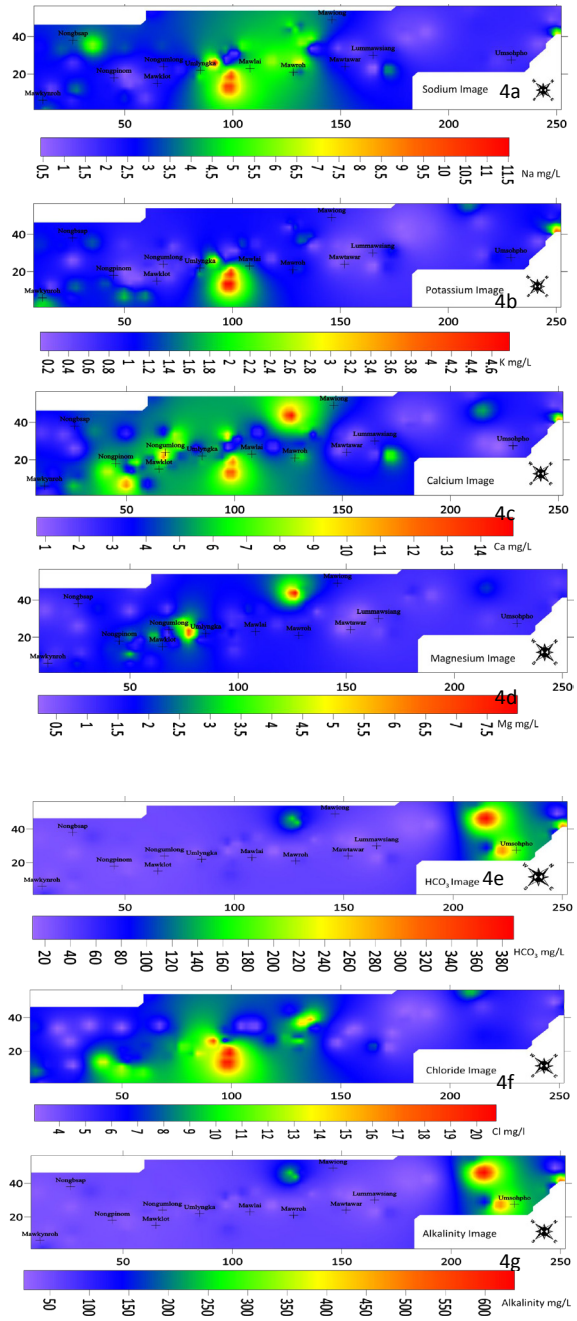

Figure 4. Cations, Anions Images. 4a: Sodium Image, 4b: Potassium Image, 4c: Calcium Image, 4d: Magnesium Image, 4e: HCO_3 Image, 4f: Cl Image, 4g: Alkalinity Image.

5.3 Trace Elements

5.3.1 Iron (Fe)

In the present study, Fe varies from 5 mg/L to 625 mg/L with an average of 107.11 mg/L (Table 3), and its spatial distribution is shown in Figure 5a. The surveyed area shows marked enrichment of Fe (178.20 times as compared to mean river water). High Fe values are seen in the area around Mawklot, Nongumlong, and west and northwest of Mawlai and Mawiong mainly in Tyrsad formations; north of Lummawsiang, and west of Umsohphoh in Barapani formations (Figure 5a). Iron is usually found in groundwater in the form of Fe^{2+}, although it can be presented as Fe^{3+}, $FeOH^{2+}$, or $FeOH^{+}$, depending on pH, oxygen content, and chemical interaction with other elements [33]. At pH values of 4.5 to 9, soluble Fe is usually in a ferrous state, especially if the medium is reducing as in most groundwater. Fe oxidizes under the action of air or by contact with chlorine, going into the ferric state, and can thus be hydrolyzed to give an insoluble iron hydroxide [34]. The Fe occurs as $Fe(OH)_2^+$, $Fe(OH)_4^-$, and $Fe(OH)_{3(aq)}$ were also observed in smaller proportions as expected, according to the pH values of this study (3.4 to 8.4 with a mean value of 6.79 in Figure 3a). $Fe(OH)_4^-$ species showed a more significant presence in sites with pH around 8.4 and positive redox potential. A criterion of 0.3 mg/L for iron is the recommended limit for domestic water supplies, primarily because of the taste threshold of iron in the water whereas for freshwater aquatic life the limit prescribed is 1 mg/L [29,35].

5.3.2 Silica Image (SiO_2)

SiO_2 varies from 3.42 mg/L to 40.43 mg/L with an average of 11.12 mg/L (Figure 5b). Hydrogen percentage plays an important role in rock weathering. The dissolution rates of most silicate minerals are independent of pH (Figure 3a) in the circumneutral region; they increase with decreasing pH in the acid region and increase with increasing pH in the alkaline region (Figure 3g). The alkaline nature of groundwater favours the dissolution of secondary minerals. A good spatial correlation between pH and silica is observed in certain areas around Mawiang-Mawlai, Nongumlong -Maklot, and Lumawsiang.

5.3.3 Zinc

Zn 0.5 ppb to 9039 ppb with an average of 98.8 ppb (Table 3). Zinc is naturally present in water. The typical zinc content in saltwater is between 0.6 and 5 parts per billion. Zinc concentrations in rivers are usually between 5 and 10 parts per billion. Very high Zn content in water is found in the area around Umsohphoh where the Zn values rise to 9039 ppb (Figure 5c). The high concentration is also observed in the area around Shillong ranging from 19 ppb-3356 ppb with an average of 552 ppb along with high Fe, and Mn values [21]. This zinc anomaly is on Barapani formation in the vicinity of Kyrdem granite and

is associated with lineaments. The area between Shillong city and Umsohphoh warrants detailed geophysical investigation for Pb-Zn mineralization.

Zinc can, however, be toxic to some species of fish at much lower concentrations than the standard limit for drinking water [36]. Sensitive species may be killed by concentrations of a few hundred micrograms per liter. Zinc solubility is affected by the temperature and pH of the water. Zinc is insoluble in water when the pH is close to neutral. With rising acidity, solubility rises. For domestic water supplies, the concentration of zinc should be below 5.0 mg/L to protect against undesirable aesthetic effects [29,35]. Zinc has a nutritional value as a trace element and is found in the human body in amounts of about 2.3 mg. Its primary roles include enzymatic reactions and DNA replication. Zinc is found in the human hormone insulin, and it plays a vital role in sexual development. A daily dose of 2 mg-3 mg is recommended to avoid deficiency. Because the human body only absorbs 20-40% of the zinc included in the diet, many individuals drink zinc-rich mineral water. Tastelessness and a loss of appetite are two symptoms of zinc deficiency. The immunological and enzyme systems of children may be harmed.

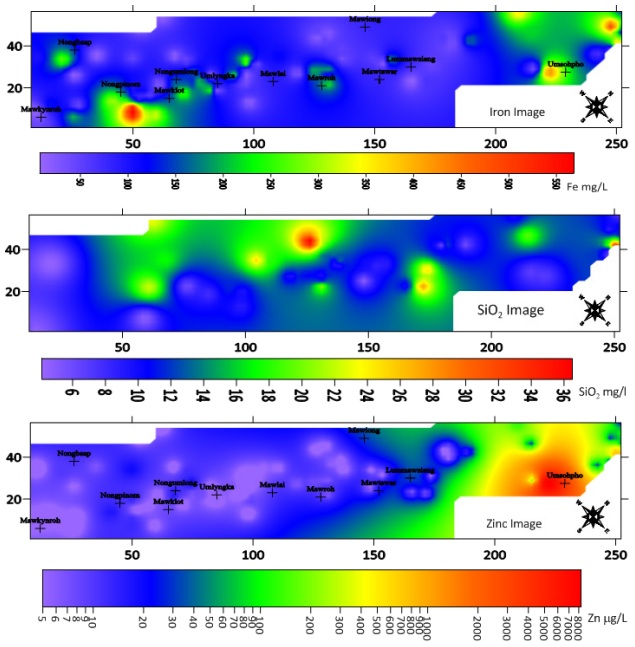

Figure 5. Trace elements Images. 5a: Iron Image, 5b: SiO_2 Image, 5c: Zinc Image

6. Hydrogeochemical Facies

The water is dominated by Ca, followed by Na > Mg > K, except in a few samples where Mg dominates (n=5samples) the cations. In anionic chemistry, the order of abundance is HCO_3 > Cl > SO_4. The major cations and anions are plotted on Piper's trilinear diagram (Figure 6a) [37].

The trends from the $CaHCO_3$ water to the $NaHCO_3$ water indicate an evolution of the water and cation exchange of Ca for Na. Dominated by Ca^{2+} and HCO_3^- derived from the weathering of minerals in the bedrock, including calcite the most easily weathered mineral in the aquifer. Low concentrations of Na^+ in the $CaHCO_3$ waters indicate little cation exchange and dissolution of Na-minerals. The $CaHCO_3$ waters represent recharge waters with short residence times. The $NaHCO_3$ water type is the most evolved of the waters and derives its Na^+ from cation exchange of Ca for Na and K as well as dissolution of plagioclase which also results in high SiO_2 [37]. $NaHCO_3$-dominated (103 samples) because of cation exchange and plagioclase, SiO_2 dissolution. Predominant silicate weathering and limited carbonate dissolution are also indicated by the Ca/Na Vs HCO_3/Na plot and Ca/Na Vs Mg/Na plots (Figure 6c, 6d). HCO_3Ca-Mg type water (only 5 samples) indicates major components of surface recharge and water-rock interaction in groundwater only limited since the area has high relief hence the water has less time to interact with country rocks. Hydrogeochemical facies mapping [38] shows that six samples belong to Ca-Mg facies, one sample to Cl-SO_4 facies, five samples to bicarbonate, fourteen samples show Ca-Na facies, six samples to Cl+SO_4+HCO_3 facies, six samples to Cl+SO_4+HCO_3 ten samples to Na-Ca, and 66 samples belong to HCO_3+Cl+SO_4 facies (Figure 6b).

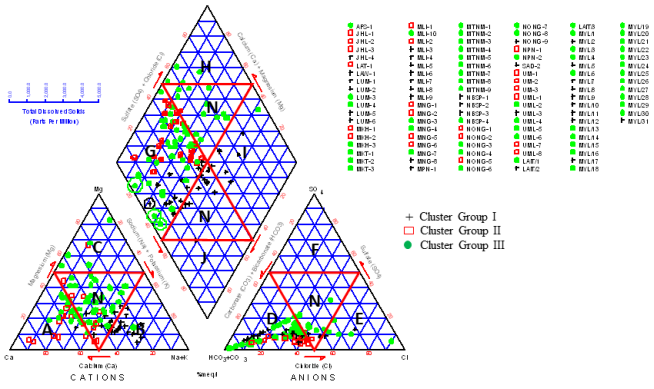

6a: Piper trilinear diagram for hydrogeochemical facies for the groundwater samples of Shillong basin [37]. A Calcium Type, B Sodium Potassium Type, C Magnesian Type, D Bicarbonate, E Chloride Type, F Sulphate Type, Type; G-Sec. Alk. (Carbonate Hardness), H-Sec. Salinity (Non carbonate Hardness), I-Primary Salinity (Noncarbonate Alk.), J-Pri. Alk. (Carbonate Alk.), N-Neutral Type

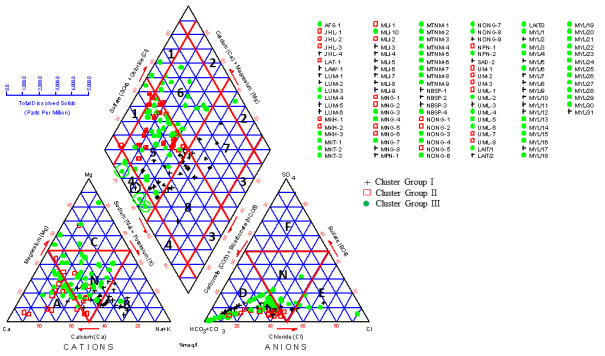

6b: Piper diagram for the facies mapping approach for stream water samples from Shillong Basin after [39]. A Calcium Type, B Sodium Potassium Type, C Magnesian Type, D Bicarbonate, E Chloride Type, F Sulphate Type, Type; G-Sec. Alk. N-Neutral Type, 1 Calcium-Magnesium, 2 Chloride-Sulphate, 3 Sodium-Potassium, 4 Bicarbonate, 5 Bicarbonate-Chloride-Sulphate, 6 Calcium-Sodium, 7 Chloride-Sulphate-Bicarbonate, 8 Sodium-Calcium

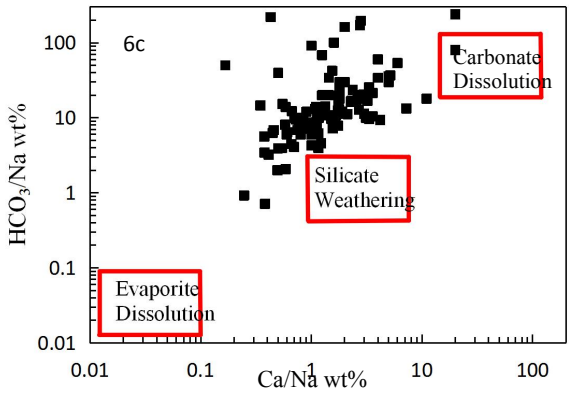

6c: Ca/Na vs HCO_3/Na

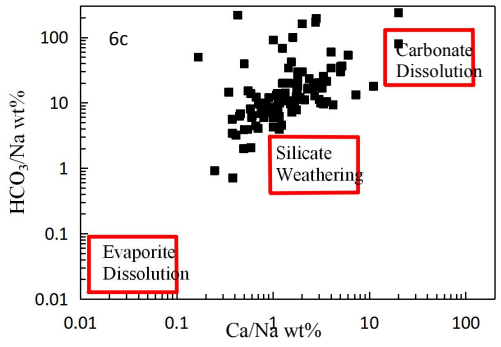

6d: Ca/Na vs Mg/Na

Figure 6. Plots showing predominace of silicate weathering and minor carbonate dissolution.

6.1 Indices of Base Exchange

Changes in the chemical composition of groundwater along its flow path can be understood by studying the Chloro-Alkaline Indices (CAI). Schoeller [40,41] suggested 2 Chloro-Alkaline Indices (CAI) 1, 2 for the interpretation of ion exchange between groundwater and the host environment. The Chloro-Alkaline Indices I are calculated from the following relations:

$$\mathbf{CAI-1} = Cl^- - \left(\frac{Na^+ + K^+}{Cl^-}\right) \quad (2)$$

The choloroalkaline indices (CAI) can be either positive or negative depending on whether the exchange of Na and K is from water with Mg and Ca in rock/soil or vice versa. If Na and K are exchanged in water with Mg and Ca, the value of the ratio will be positive, indicating a base exchange phenomenon. The negative values of the ratio will indicate chloroalkaline disequilibrium and the reaction as a cation-anion exchange reaction [41]. In the present case, 89% values (96 No.) are negative ranging from 0.00 to -3.525 (Cation-anions exchange), and 11% values (12 No.) are positive ranging from up to 0 to +0.808 i.e., showing a slight base exchange phenomenon in the area around Nongpinom and Umlyngka (Table 3). The result suggests that cation exchangeable is primarily the main mechanism responsible for the chemical composition of the groundwaters in the studied area (Figure 7c).

6.2 Normalized Mg

In particular, the magnesium enrichment associated with intense and pervasive chlorite alteration that accompanies the four known deposits is reflected in the major element composition of groundwaters from the vicinity of each known deposit. Mg^{2+} is very much more than Ca^{2+} and $Na^+ + K^+$ in the areas of magnesium metasomatic alteration. NMg can be used as a hydrogeochemical exploration indicator for uranium deposits. This can be determined by Normalised Mg^{2+} and is expressed as NMg as follows:

$$\text{NMg} = \frac{Mg^{2+}}{Ca^{2+} + Mg^{2+} + Na^+ + K^+} \quad (3)$$

All values in meq/L [42]. The NMg varies from 0.048 to 0.83 with an average of 0.23 (Figure 7b). In general, NMg values are <0.8 indicating that they are collected from non-Mg metasomatic areas i.e., nonmineralized aquifers. However, one sample collected from the Mawklot area (MKT-1) shows a 0.83 NMg value showing Mg metasomatism. This zone coincides with high Ra(eU_3O_8) = 2 to 4 ppm, Ra(eU_3O_8)/K = 2-7 × 10^{-4} & ThO_2/K = 10-15 × 10^{-4}. NMg shows weak positive correlations with Mg

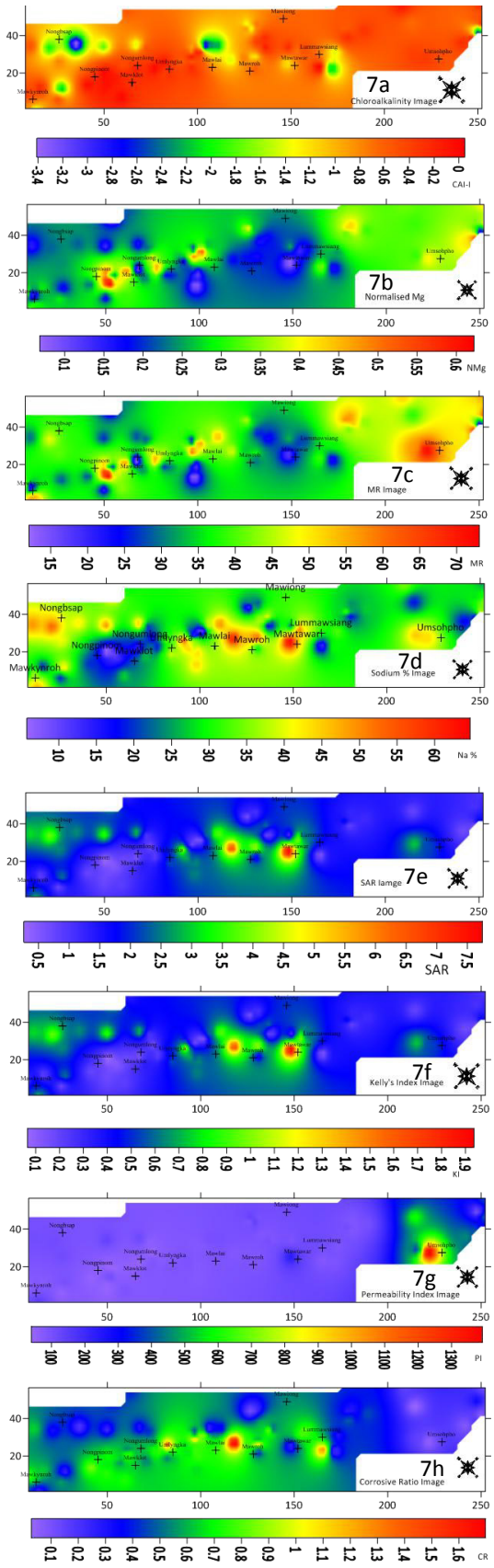

Figure 7. Calculated Water Quality Images. 7a: Chloroalkalinity Image, 7b: NMg, 7c: MR, 7d: %Na, 7e: SAR, 7f: Kelly's Index, 7g: Permeability Index, 7h: Corrosive ratio Image.

(0.29), HCO_3 (0.22), pH (0.33), Alk (0.23) and Zn 90.22). NMg shows strong negative correlations with Na (–0.62) and weak negative correlations with K (–0.42), Ca (–0.32), Cl (–0.33), TDS (–0.34), and cond. (–0.35) in Table 4. The radiometric surveys in the area resulted in locating two low-intensity uranium anomalies (Figure 1). Medium to high order radioactivity was recorded in ironstone over an extension of 100 m × 50 m around 1.5 km northwest of Nongkseh (Lat: –25°34'56.6", Long: –91°51'28.1"), The rock samples analyzed 0.022% to 0.046% eU_3O_8, < 0.010% to 0.017% U_3O_8, 0.040% to 0.089% ThO_2 and < 0.005% to 0.005% Ra(eU_3O_8). It occurs as floats on the surface of the soil which is a natural phenomenon. This radioactive anomaly is nearer to the unconformity and nonradioactive away from the unconformity. The data indicates the mixed nature of the anomaly. The high content of ThO_2 is due to the presence of radioactive heavy mineral resistates like monazite and sphene in the rock. Another low order radioactivity was recorded in graphite schist over 10 m × 2 m around 1 km NNE of Nongumlong on the way to Umiam river analyzing 25 ppm eU_3O_8, 16 ppm ThO_2, 10 ppm Ra (eU_3O_8) (Lat: – 25°34'15", Long: – 91°50'08" Figure 1). After 10 m away along with the same road section low order radioactivity was also recorded in chloritic phyllite over an extension of 100 m × 2 m analyzing 14 ppm to 30 ppm eU_3O_8, 11 ppm to 26 ppm ThO_2, and 3 ppm to 8 ppm Ra (eU_3O_8). Spatial association of low order anomalies and Mg metasomatism warrants subsurface investigations for uranium mineralization possibilities.

6.3 Magnesium Ratio (MR)

In most water bodies, calcium and magnesium are in a condition of balance. More magnesium in the water reduces crop output. Because the study area's rocks are primarily Arenites and Phyllites, with some basic and conglomerate strata, the majority of the water has more calcium than magnesium. The magnesium ratio was determined using the following equation:

$$\text{MR} = \frac{Mg^{2+}\, x\, 100}{Ca^{2+} + Mg^{2+}} \quad (4)$$

The MR values vary from 5.96 to 97.06 with an average of 130.09 (Table 3). The high values are observed in the area around Umsohphoh and along the unconformity as small circular anomalies but it constitutes very small areas, while predominantly the study area has lower MR values (Figure 7c). The 88 samples (81.48%) show <50% values i.e., suitable for irrigation purposes while 20 samples (18.52%) show >50% values and is not suitable irrigation purposes (Table 3).

6.4 Sodium Percentage

Sodium is an essential ion for irrigation water classification because it inhibits permeability, given its reactivity with soil. The %Na is computed as:

$$\%\text{Na} = \left(\frac{Na+K}{Ca+Mg+K+Na}\right) X\ 100 \quad (5)$$

where all ionic concentrations are expressed in meq/L. According to Wilcox [43], in all-natural waters, $\%Na^+$ is a common parameter to assess its suitability for irrigation purposes as shown in Table 2. Na^+ ions are absorbed by clay particles when the concentration of Na+ in irrigation water is high, displacing Mg^{2+} and Ca^{2+} ions. This exchange of Na+ in water for Ca^{2+} and Mg^{2+} in soil lowers the permeability of the soil and eventually leads to poor internal drainage, resulting in hard soils when dry [44,45]. The values of $\%Na^+$ of the study area vary from 2.19% to 69.63% with an average value of 34.94% (Table 2, Figure 7d) which falls in the excellent (27 samples 25%) to good category (40 samples 37.04%), showing that the groundwater of the study area is suitable for drinking as well as irrigation; meanwhile, 34 samples (31.48%) are permissible and 7samples (6.48%) are doubtful while none samples are unsuitable category (Table 3). The EC ranges between 5.0 µS/cm and 284.0 µS/cm, in which the groundwater is excellent to a good category in Figure 8; therefore, the groundwater can be useful for irrigation.

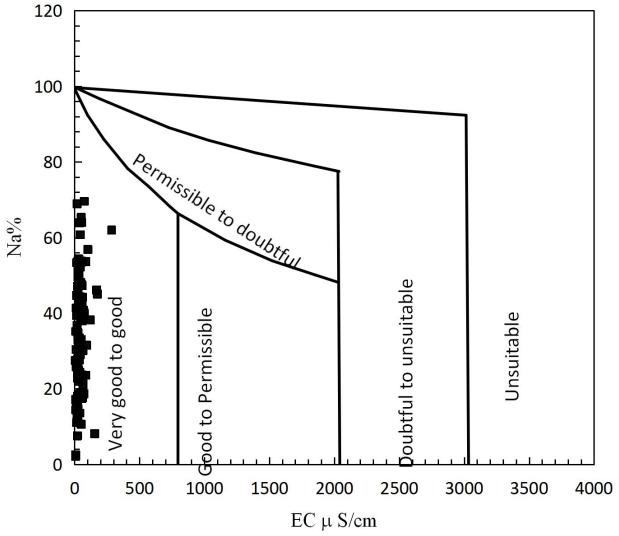

Figure 8. Electrical conductivity vs. %Na plot after [43]

6.5 Sodium Adsorption Ratio (SAR)

Sodium adsorption ratio (SAR) is a measure of the alkali or sodium hazard to crops. When the sodium concentration is high, sodium ions tend to become adsorbed onto the clay soil particles, displacing Mg^{2+} and

Ca^{2+} ions. Exchange of Na^{+} for Ca^{2+} and Mg^{2+} results in soil with poor internal drainage and restricted circulation of air and water when wet. Such soils usually form hard and unmanageable clods when dry, SAR is defined as [43,44]:

$$\mathbf{SAR} = \frac{\mathbf{Na}}{\sqrt{(\mathbf{Ca+Mg})/2}} \quad (6)$$

where all ionic concentrations are expressed in meq/L. The SAR of the study area ranges between 0.066 and 8.514, with an average value of 2.074 (Table 2, Table 5; Figure 7e) which indicates that no alkalinity hazard is anticipated in the study area and the EC ranges between 5.0 µS/cm and 284.0 µS/cm, in which the groundwater classifies as excellent to a good category in Figure 9. Most of the samples fall into the C_1S_1 category (Low salinity and low sodium) of waters requiring good drainage [46]. Crops with good salt tolerance should be selected; gypsum amendments make it possible to use this water while only two samples are in the C_2S_1 field (Figure 9). Therefore (medium salinity and low sodium), based on the sodium hazard class the groundwater of the study area is suitable for irrigation. SAR values greater than 6 to 9, the irrigation water could be expected to cause a permeability problem on shrinking and swelling types of clayey soils which are observed in the north of Mawlai and SW of Mawtawar villages (Figure 7e).

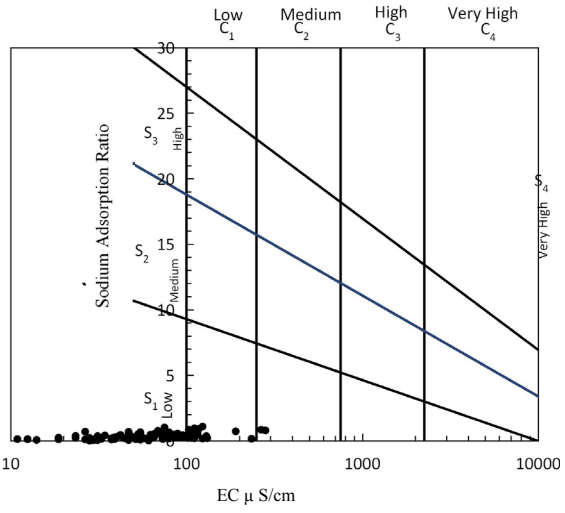

Figure 9. Diagram for USSL classification of irrigation water after [48]

6.6 Kelly's Index

Kelly's Index (KI) is used for the classification of water for irrigation purposes [47]. KI is calculated by the following formula; where ions are expressed in meq/L.

$$\mathrm{KI} = \frac{Na^{+}}{(Ca^{2+} + Mg^{2+})} \quad (7)$$

KI (>1) shows an excess of sodium and KI (<1) signifies its deficit in waters [48]. A Kelly's ratio of more than one indicates excessive sodium in water. Therefore, water with Kelly's index less than one is suitable for irrigation, while those with a ratio of more than one is unsuitable (12.96%). The KI varies from 0.016 to 2.13 with an average value of 0.52 (Table 2). In the present study, 12.96% of the water samples are unsuitable for irrigation with more than one KI is in the NW of Mawlai and SW of Mawtawar villages (Figure 7f). While 87.04% are suitable for irrigation which shows KI<1 (Table 4, Figure 7f).

6.7 Permeability Index (PI)

The salt, calcium, magnesium, and bicarbonate concentrations in soil impact soil permeability, which also affects the quality of irrigation water over time. Doneen [49] has evolved a criterion for assessing the suitability of water for irrigation based on PI, calculated by using the formula:

$$PI = \frac{Na^{++} + \sqrt{HCO3^{-}}}{Ca^{++} + Mg^{++} + Na^{+}} \times 100 \quad (8)$$

where all the ions are expressed in meq/L. PI ranges from 28.59 to 1493.33 with averages of 130.09 (Table 2). According to PI values, the groundwater 3 samples fall in class I, 32 samples in Class II, and the rest 73 samples (67.6%) plot in Class III. Class I and Class II waters are categorized as good for irrigation with 75% or more of maximum permeability (Figure 10; Figure 7g). Class III waters are unsuitable with 25% of maximum permeability [49]. Very high values are seen near the Umsohpho area which coincides with the Zn anomaly area also in Figure 5c.

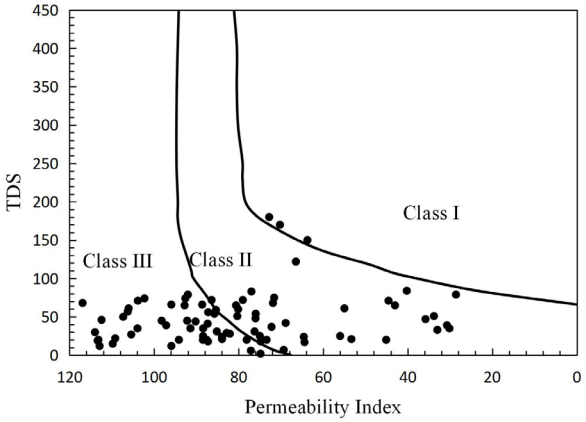

Figure 10. PI vs TDS plot for water samples after [49]

6.8 Corrosivity Ratio (CR)

The corrosivity ratio is defined by the following formula after [50]:

$$CR\ \frac{\left(\frac{Cl^-}{35.5}\right)+2\left(\frac{SO_4^-}{96}\right)}{2\left\{\frac{(HCO_3^-+CO_3^-)}{(100)}\right\}} \quad (10)$$

where all the ions are expressed in ppm (Table 3). The vales vary in the study area from 0.02 mg/L to 16.90 mg/L with an average of 0.76 mg/L (Figure 7h). The CR denotes the potential for groundwater to induce corrosion of pipes and is expressed as the ratio of alkaline earth to saline salts in groundwater. Corrosion can result in the loss of hydraulic capacity of pipes. In the area SW of Umlingka, N of Mawlai, and SE of Lummawsiang where the CR value >1, polyvinyl chloride (PVC) pipes should be used (Table 3, Figure 7h). Most of the area under investigation shows CR <1 (Figure 7h) where galvanized pipes can be used.

7. Statistical Analysis and Unsupervised Classification

Correlation matrix of all the hydrogeochemical data (Table 4) shows positive correlation of conductivity with TDS (0.93) Ca (0.92), Na (0.81), K (0.73), Cl (0.62), Mg (0.54), TH (0.56) and SiO_2 (0.47). TDS indicated high positive correlations with Ca (0.73), Mg (0.73), and conductivity (0.56) and moderate positive correlations with HCO_3 (0.48) and Alkalinity (0.48). pH indicated negative correlations with all the parameters. Na indicated positive correlations with K (0.76), Ca (0.67), Cl (0.64), TDS (0.74), Conductivity (0.81) and negative with NMg (-0.62). Ca has positive correlations with K (0.62), Mg (0.62), TDS (0.65), Conductivity (0.73), SiO_2 (0.65) and TH (0.73). Uranium and SO_4 contents are constant for the entire area of the investigation except for three values so not considered for statistical analysis. The hydrogeochemical data was standardized (X-μ/σ) for unsupervised classification which forms a part of Machine learning for data mining.

7.1 Cluster Analysis

The physicochemical parameters, anions, cations, and trace elements similarity between objects was measured by squared Euclidean distances, and Ward's method of divisive agglomerative hierarchical clustering (AHC) method was used for cluster analysis [51]. The dendrogram prepared based on the cluster analysis shows three distinct classes /groups. Group-I consists of Na, K, Cl, TDS, and conductivity. It contains TDS and conductivity along with three independent variables Na, K, and Cl, indicating that the TDS has contributions due to Conductivity, Na, K, and Cl. Group II consists of HCO_3 and Alkalinity. HCO_3 and Alkalinity are closely related to other independent variables Zn and SiO_2 and Group I consist of TDS conductivity with PS and CR (Figure 11a, 11b) and Group III consists of TH Mg and Ca with two independent variables as Fe, pH, (Figure 11a, b). Group-II in Figure 11b consists of a very low linkage of KR and SAR with %Na. Group-III consists of MR, and PI with CAI-I at some distance. The spatial distribution of these groups, in general, is as under:

1) South of Mawlai all the three groups of waters are found granites and its vicinity area, TH moderate to high. Low conductivity. In the case of water quality parameters also the same pattern is seen (Figure 11e).

2) From Mawlai to Lummawsiang Group I and III are found mixed TDS moderate to high. TH Moderate to high. Moderate to high conductivity. This zone has all three groups but in Group II only six samples fall along with the group I and III.

3) Further northwards from north of Lummawsiang to the extreme northern end of the investigated area only group III water is found. In general, these areas have low TDS, TH low, and low conductivity. All the samples that fall in this area are of group III only.

Various groups of water samples are also depicted in Figure 6a and 6b in the piper's diagram.

7.2 Factor Analysis

Factor analysis is one of the most important statistical tools for interpreting ground-water hydrogeochemistry. pH, EC, TDS, TH, Alkalinity, Na, K, Ca, Mg, Cl, HCO_3, SiO_2, Fe, and Zn were the variables included in factor analysis. All the factors showing >1.0 eigenvalues are considered significant based on the scree test. Factors were analyzed based on strong, moderate, and weak loadings according to the total values of >0.75, 0.75 to 0.5, and 0.5 - 0.3. These categories are used to characterize the significance of factors. The first factor explains 33.75% variability and second is 16.44% and the third is 10.7%, cumulative the three factors account for 68.88% variability. The first factor shows strong loadings for Cond, TDS, Na, and Ca, moderate positive loadings for TH, K, and Cl, and weak positive loadings for alkalinity, HCO_3, SiO_2, Mg, and Fe, almost all are showing positive loading of varying amounts thus it can be accounted for TDS and conductivity (Figure 12a). The second factor shows weak positive loadings for Na, K Cl, TDS, and conductivity; strong negative loadings for HCO_3, Alkalinity and weak negative loading for Zn, and. The third factor shows weak positive loading for Zn, Alkalinity, and HCO_3 whereas, strong negative loading for TH and weak to moderate negative loadings for pH, Mg, and Ca (Table 5) thereby indicating Zn variation along with alkalinity and bicarbonate variation in water (Figure 12b). The factor oblimin rotation shows that the first D_1 axis shows positive loading for all the ions with

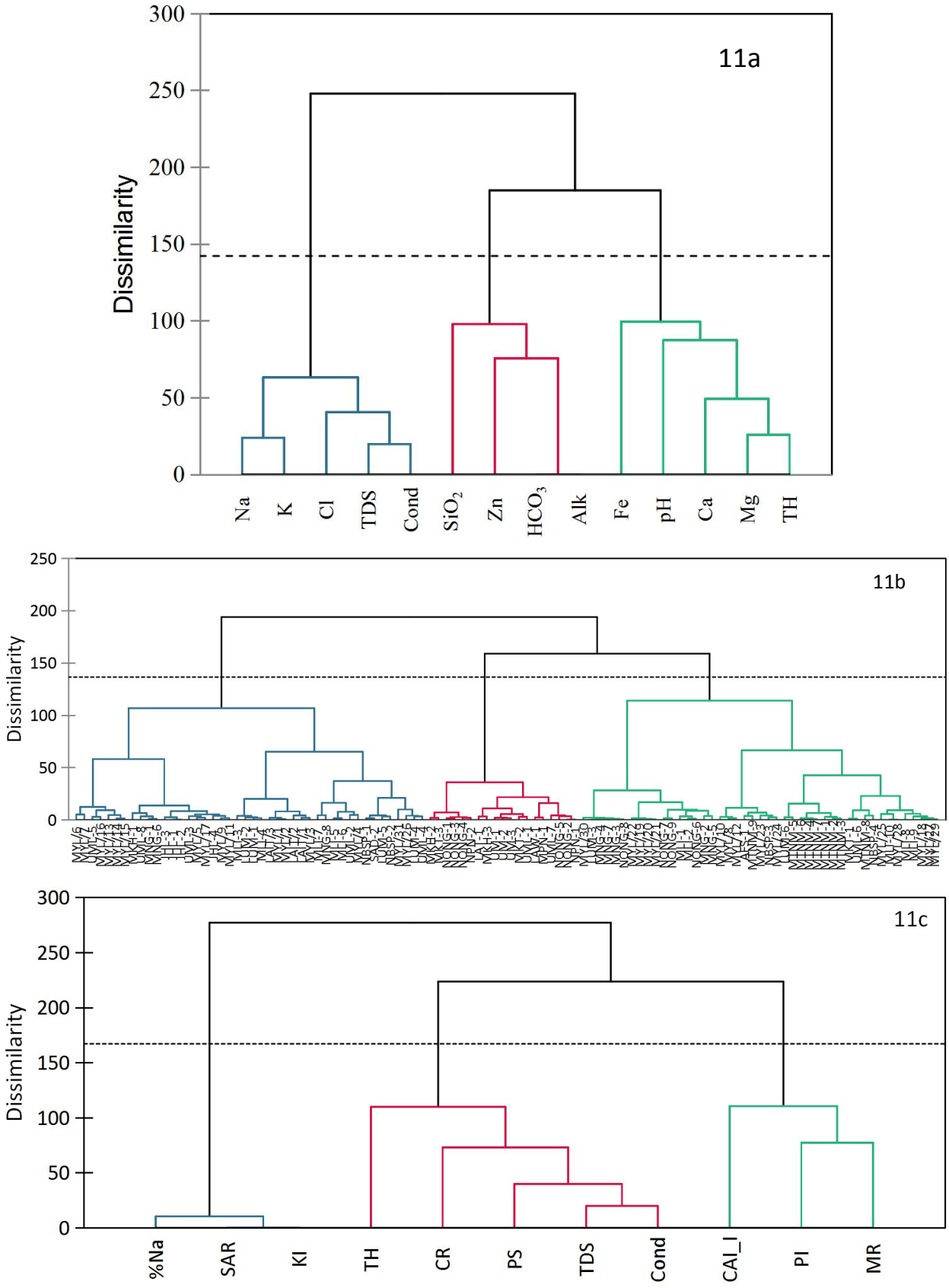
11a
Dissimilarity
300
250
200
150
100
50
0
Na
K
Cl
TDS
Cond
SiO2
Zn
HCO3
Alk
Fe
pH
Ca
Mg
TH
11b
Dissimilarity
250
200
150
100
50
0
11c
Dissimilarity
300
250
200
150
100
50
0
%Na
SAR
KI
TH
CR
PS
TDS
Cond
CAI_I
PI
MR

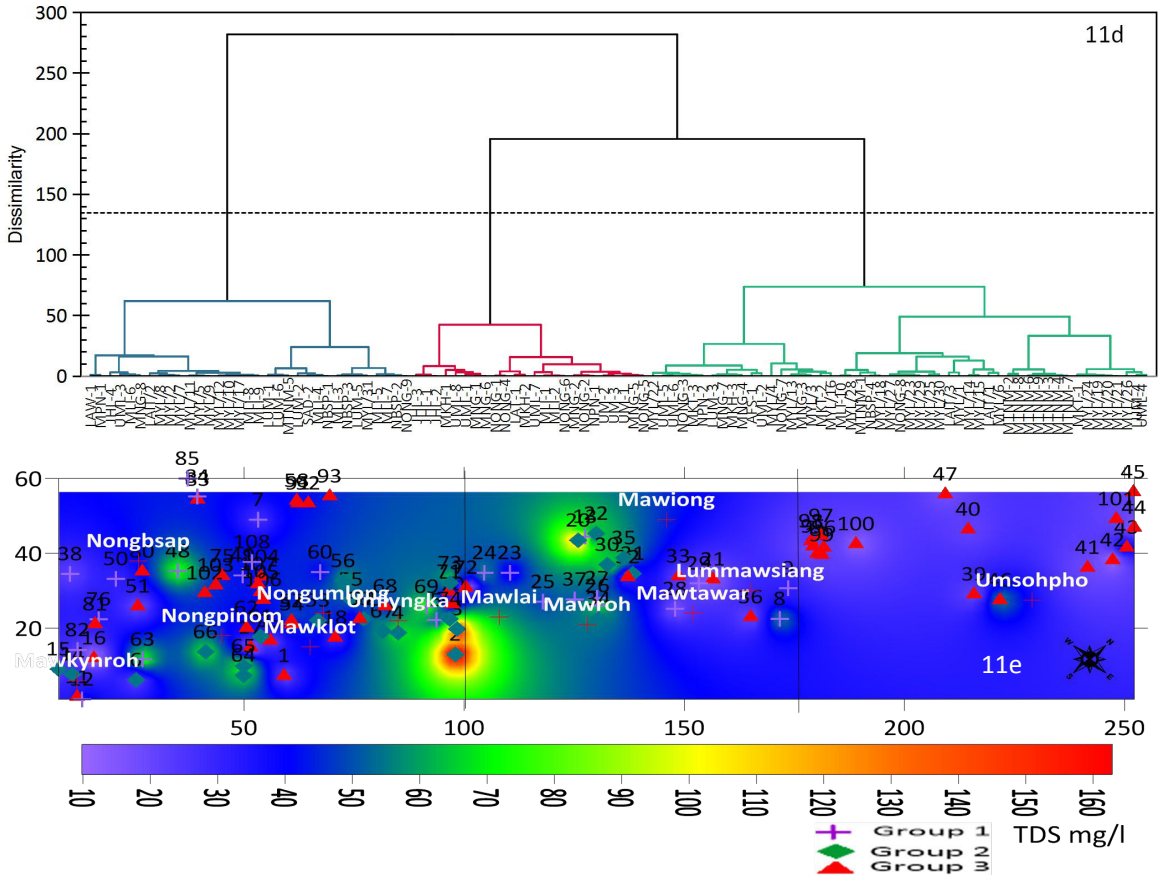

Figure 11. Dendrogram of hydrogeochemical parameters using ward's method. 11a: Dendrogram based on columns and; 11b: Dendrogram based on rows; 11c based on columns (Water Quality parameters), 11d: based on rows, 11e: Cluster groups of water overlayed on TDS clearly showing the spatial dispositions.

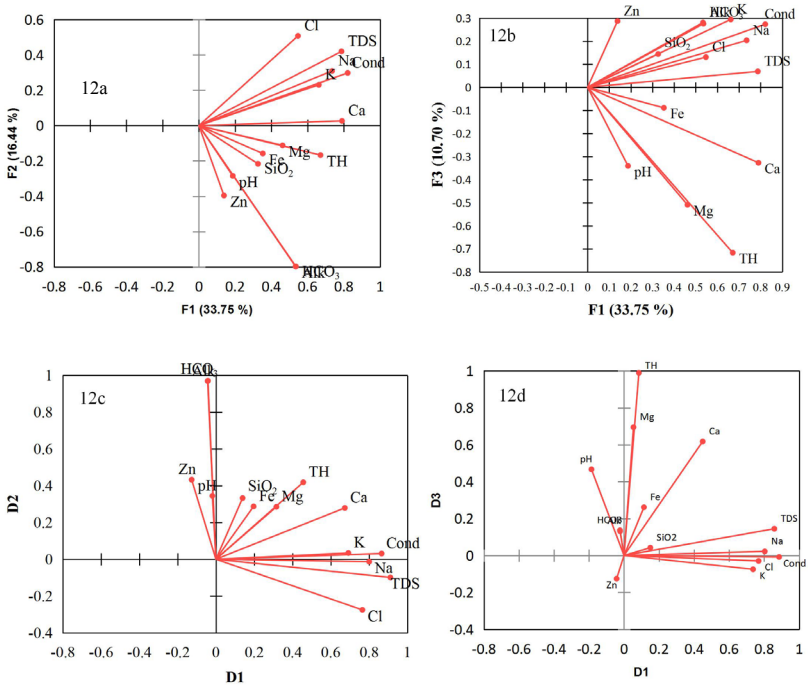

Figure 12. 12a: loading biplot of F1 vs F2 explains 50.19%; 12b: F1 vs F3 biplot explains 44.45%. 12c: Factor loading after oblimin rotation D1 vs D2 biplot; 12d: D1 vs D3 biplot

exception of Zn, Alkalinity, and HCO_3. D_2 axis shows +ve loadings for Zn Alkalinity and HCO_3 (Figure 12c). D_3 axis shows high loading for TH, Ca, Mg and weak loading for pH thereby indicating TH variation (Table 6, Figure 12d).

Table 5. Factor analysis of hydrogeochemical parameters of the study area.

Factor pattern	F1	F2	F3	F4	Final communality
Na	**0.735**	0.310	0.203	0.122	0.693
K	**0.662**	0.231	0.294	0.012	0.578
Ca	**0.790**	0.027	–0.327	0.125	0.747
Mg	0.462	–0.112	**–0.509**	–0.015	0.485
Cl	**0.547**	0.508	0.131	–0.284	0.655
HCO_3	0.536	**–0.798**	0.275	0.016	**1.000**
Fe	0.353	–0.158	–0.089	**–0.496**	0.403
TDS	**0.787**	0.420	0.069	0.046	0.803
pH	0.187	–0.285	**–0.341**	0.146	0.254
Cond.	**0.821**	0.298	0.273	0.035	0.840
Alk.	0.533	**–0.798**	0.281	0.013	**1.000**
TH	**0.671**	–0.167	**–0.717**	–0.085	**1.000**
SiO_2	0.326	–0.216	0.144	**0.422**	0.352
Zn	0.138	**–0.396**	0.287	–0.335	0.371
Eigenvalue	**4.725**	**2.301**	**1.497**	0.681	
Variability (%)	**33.750**	**16.436**	**10.695**	4.867	
Cumulative %	**33.750**	**50.187**	**60.882**	65.749	

Values in bold correspond for each variable to the factor for which the squared cosine is the largest

Table 6. Factor pattern after Oblimin rotation

	D1	D2	D3
Na	**0.804**	0.070	0.022
K	**0.737**	0.166	–0.075
Ca	0.449	0.014	**0.618**
Mg	0.054	–0.070	**0.695**
Cl	**0.768**	–0.187	–0.030
HCO_3	–0.023	**0.961**	0.137
Fe	0.114	0.178	**0.261**
TDS	**0.858**	–0.083	0.145
pH	–0.186	0.091	**0.467**
Cond	**0.885**	0.143	–0.008
Alk	–0.022	**0.963**	0.131
TH	0.085	–0.084	**0.989**
SiO_2	0.150	**0.351**	0.042
Zn	–0.042	**0.527**	–0.126

Values in bold correspond for each variable to the factor for which the squared cosine is the largest

8. Conclusions

The hydrogeochemical evaluation of the area suggests that the pH is acidic to alkaline. All ionic concentrations fall below acceptable WHO and ISI limits (except iron) and are found suitable for drinking. The area around Mawklot, Nongumlong, and west and northwest of Mawlai and Mawiong, largely in Tyrsad formations; north of Lummawsiang and west of Umsohphoh, mainly in Barapani formations, has high Fe content in water, which needs to be treated to make it drinkable. Water is $CaHCO_3$, $NaHCO_3$, and $CaMgHCO_3$. $CaHCO_3$ waters represent recharge waters with short residence times due to high relief of the draining area, $NaHCO_3$ water indicates an evolution of the water and cation exchange of Ca for Na due to plagioclase feldspar and silica dissolutions. Secondary mineral dissolution is observed in areas around Mawioang-Mawlai, Nongumlong-Maklot, and Lumawsiang. $CaMgHCO_3$ is characteristic of freshly recharged groundwater from precipitation. The groundwater indices of Sodium Percent (%Na), Kelley's Index (KI), Sodium Adsorption Ratio (SAR), Magnesian Ratio (MR), Electrical Conductivity (EC), Total Dissolved Solids (TDS), USSL, and Wilcox index were evaluated and found to be suitable for agro-industrial uses. Normalized Mg (NMg) shows areas of magnesium metasomatic alteration zones around the Mawklot area. Permeability Index (PI) is found to be suitable in most areas and Corrosivity Ratio (CR) shows galvanized pipes to be used for water supply.

Unsupervised classification clearly shows three groups of cations, anions trace elements, and physicochemical parameters. AHC analysis also shows three groups having similar properties that are Group I consists of Na, K, Cl, TDS and conductivity, PS, and CR. Group II consists of HCO_3 and Alkalinity, HCO_3 and Alkalinity are closely related to other independent variables Zn and SiO_2, with the very low linkage of KR and SAR with %Na. Group III consists of TH Mg and Ca with two independent variables as Fe, pH, and MR, PI with CAI-I at some distance.

The factor analysis also indicated three major groups of the hydrogeochemical parameters. Thus, clearly defining the dimensionality of water types and their spatial distribution. All the three groups type of waters found the lithological preferences i.e., Barapani Arenite, Barapani Arenites contact with Mylliem granite, Tyrsad Argilllites, and intervening Graphitic schists along the unconformity contacts in the southern part has all the three groups of waters. Followed by marginal exposures of Tyrsad Argillites, unconformity contact, and Barapani Arenites middle zone where the group II and III diminishes while at

the northernmost part with Barapani Arenite and Krydem granite contact zone has only group III type of waters. The area is devoid of uranium anomalies, except for the two low-order radioactive anomalies near NW of Nongkseh, and the spatial association of the Mg metasomatic alteration zone warrants subsurface exploration.

Acknowledgments

The author is thankful to Atomic Minerals Directorate for Exploration and Research (AMD) Northeastern Region (NER) Shillong for providing logistics and Chemistry laboratory AMD NER analytical facilities for water samples.

Conflicts of Interest

The author declares no conflicts of interest regarding the publication of this paper.

References

[1] Piron, E., Accominotti, M., Domard, A., 1997. Interaction between Chitosan and Uranyl Ions. Role of Physical and Physicochemical Parameters on the Kinetics of Sorption. Langmuir. 13(6), 1653-1658. DOI: https://doi.org/10.1021/la960765d

[2] Cumberland, S.A., Douglas, G., Grice, K., et al., 2016. Uranium mobility in organic matter-rich sediments: A review of geological and geochemical processes. Earth Science Reviews. 159, 160-185. DOI: https://doi.org/10.1016/j.earscirev.2016.05.010

[3] Stanley Dovie, M., Wilkin Richard, T., 2019. Solution equilibria of uranyl minerals: Role of the common groundwater ions calcium and carbonate. Journal of Hazardous Materials. 377(5), 315-320. DOI: https://doi.org/10.1016/j.jhazmat.2019.05.101

[4] Sanford, R.F., Pierson, C.T., Crovelli, R.A., 1993. An objective replacement method for censored geochemical data. Math Geology. 25, 59-80.

[5] De Caritat, P., Kirste, D., 2005. Hydrogeochemistry — clues to hidden mineralization, AusGeo News. 77, 5.

[6] De Caritat, P., Lech, M., Jaireth, S., et al., 2005b. Riverina Geochemical Survey - A National First. AusGeo News. 78, 6.

[7] Barooah, B.C., Goswami, I.D., 1972. Precambrian stratigraphy of the Assam plateau. Journal of Mines, Metals and Fuels. 20, 368-373.

[8] Mazumdar, S.K., 1986. The Precambrian Framework of Part of Khasi Hills, Meghalaya. Records Geology Survey India. 117(2), l-59.

[9] Ahmed, M., 1981. Stratigraphic Class of Shillong Group, Khasi Hills, Meghalaya. Journal of Mines, Metals and Fuels. pp. 295-297.

[10] Bhattacharjee, C., Rahman, S., 1985. Structure and lithostratigraphy of the Shillong Group of rocks of East Khasi Hills of Meghalaya. Bulletin of Geological Mining and Metallurgical Society India. 53, 90-99.

[11] Acharyya, S.K., Mitra, N.D., Nandy, D.R., 1986. Regional geology and tectonic setting of Northeast India and adjoining region. Memoirs of the Geological Survey of India. 119, 6-12.

[12] Ghosh, S., Chakraborty, S., Bhalla, J.K., et al., 1991. Geochronology and geochemistry of granite plutons from East Khasi Hills, Meghalaya. Journal of the Geological Society of India. 37, 331-342.

[13] Ghosh, S., Chakraborty, S., Paul, D.K., et al., 1994. New Rb-Sr isotopic ages and geochemistry of granitoids from Meghalaya and their significance in middle-to-late Proterozoic crustal evolution Indian Minerals. 48(1&2), 33-44. Geoscience. 11, 1-16.

[14] Biswas, S., Isabelle, C., Grujic, D., et al., 2007. Exhumation and uplift of the Shillong Plateau and its influence on the eastern Himalayas: New constraints from apatite and zircon (U-Th- [Sm])/He and apatite fission track analyses: Tectonics. 26, TC6013. DOI: https://doi.org/10.1029/2007TC002125

[15] Mitra, S.K., 1998. Structural history of the rocks of the Shillong Group around Sohiong, East Khasi Hills district, Meghalaya. Indian Journal of Geology. 70(1&2), 123-131.

[16] Nandy, D.R., 2001. Geodynamics of NE India and the adjoining region; ACB publication. pp. 209.

[17] Yin, A., Dubey, C.S., Webb, A.A.G., et al., 2010. Geologic correlation of the Himalayan orogen and Indian craton: Part 1. Structural geology, U-Pb zircon geochronology, and tectonic evolution of the Shillong Plateau and its neighboring regions in NE India. GSA Bulletin. 122(3/4), 336-359. DOI: https://doi.org/10.1130/B26460.1

[18] Dhurandhar, A.P., 2020. Lithostructural mapping of Proterozoic Shillong basin Meghalaya. Unpub. Rept. Orion Geohytech India.

[19] Climate and Weather data on Shillong India, 2019. https://en.climate-data.org/asia/india/ meghalaya/ shillong-24618/#climate-graph

[20] Central Ground Water Board Northeastern Region, 2013. Aquifer Systems of Meghalaya.

[21] Jain, C.K., Sharma, S.K., Singh, S., 2021. Assessment of groundwater quality and determination of hydrochemical evolution of groundwater in Shillong, Meghalaya (India). SN Applied Sciences. 3, 33. DOI: https://doi.org/10.1007/s42452-020-03993-4

[22] Brown, E., Skougstad, M.W., Fishman, M.J., 1970.

Methods for collection and analysis of water samples for dissolved minerals and gasses. Geological SurveyTechniques of Water-Resources Investigations. TWI5-Al, 160.

[23] Woods, W.W., 1981. Guidelines for collection and field analysis of groundwater samples for selected unstable constituents. Geological Survey Techniques of Water-Resources Investigations. pp. 24.

[24] Farnham, I.M., Stetzenbach, K.J., Singh, A.K., et al., 2002. Treatment of non-detects in multivariate analysis of groundwater geochemistry data. Chemometrics & Intelligent Laboratory Systems. 60, 265-281.

[25] Cüneyt, D.G., Thyne, G., McCray, J.E., et al., 2001. Evaluation of graphical and multivariate statistical methods for classification of water chemistry data. Hydrogeology Journal. 10, 455-474.

[26] Sanford, R.F., Pierson, C.T., Crovelli, R.A., 1993. An objective replacement method for censored geochemical data. Math Geology. 25, 59-80.

[27] World Health Organization, 2011. Guidelines for Drinking-Water Quality. 4th Edition, Incorporating the First Addendum, Geneva. pp. 564.

[28] Leybourne, M.I., Cameron, E.M., 2010. Ground Water in geochemical exploration. Geochemistry Exploration Environment Analysis. 10(2), 99-118.

[29] McKee, J.E., Wolf, H.W., 1963. Water quality criteria. Calif St. Cent Bd., Publ. No. 3A, 548.

[30] Code of Federal Regulations, 1983. Title 40, Protection of Environment, Part 143: National secondary drinking water regulations, 293. Government Printing Office, Washington, D.C.

[31] Rose, S., 2002. Comparative major ion geochemistry of piedmont streams in the Atlanta, Georgia region: possible effects of urbanization. Environmental Geology. 42, 102-113.

[32] Leybourne, M.I., Cameron, E.M., 2010. Ground Water in geochemical exploration. Geochemistry Exploration Environment Analysis. 10(2), 99-118.

[33] National Academy of Sciences, National Academy of Engineering, 1974. A report of the committee on water quality criteria 1972 U.S. Government printing office Washington D.C.

[34] Ruiz, Á., Cuenca, Á., Agila, R., et al., 2019. Hydrochemical characterization of groundwater in the Loja Basin (Ecuador). Applied Geochemistry. 104, 1-9.

[35] Okan, Ö.Ö., Kalender, L., Çetindag, B., 2018. Trace-element hydrogeochemistry of thermal waters of Karakoçan (Elazıg) and Mazgirt (Tunceli), Eastern Anatolia, Turkey. Journal of Geochemical Exploration. 194, 29-43.

[36] Nelson Eby, G., 2004. Principles of Environmental Geochemistry, Chapter 4, Brooks/Cole. Waveland Press Inc. USA. pp. 514.

[37] Piper, A.M., 1944. A graphic procedure in the geochemical interpretation of water analysis. Eos Transactions American Geophysical Union. 25, 914-923.

[38] Lipfert, G., Reeve, A.S., Sidle, W.C., et al., 2006. Geochemical patterns of arsenic-enriched groundwater in fractured, crystalline bedrock, Northport, Maine, USA. Applied Geochemistry. 21, 528-545.

[39] Back, W., 1961. Techniques for mapping of hydrochemical facies. USGS Professional Paper 424-D. pp. 380-382.

[40] Schoeller, H., 1965. Qualitative evaluation of groundwater resources. In: Methods and techniques of groundwater investigation and development. Water resources series no. 33. UNESCO. pp. 44-52.

[41] Schoeller, H., 1977. Geochemistry of groundwater. In: Groundwater studies- an international guide for research and practice. UNESCO, Paris. 15, 1-18.

[42] Giblin, A.M., Snelling, A.A., 1983. Application of hydrogeochemistry to uranium exploration in the Pine Creek Geosyncline, Northern Territory, Australia. In: G.R. Parslow (Editor), Geochemical Exploration 1982. Journal of Geochemical Exploration. 19(1-3), 33-55.
DOI: https://doi.org/10.1016/0375-6742(83)90006-7

[43] Wilcox, L.V., 1955. Classification and use of irrigation waters. USDA Circular 969, Washington D.C.

[44] Todd, D.K., 1980. Groundwater hydrology, 2nd Ed. Wiley, New York.

[45] Collins, R., Jenkins, A., 1996. The Impact of Agricultural Land Use on Stream Chemistry in the Middle Hills of the Himalayas, Nepal. Journal of Hydrology. 185, 71-86.
DOI: http://dx.doi.org/10.1016/0022-1694(95)03008-5

[46] Ali, S.A., Ali, U., 2018. Hydrochemical characteristics and spatial analysis of groundwater quality in parts of Bundelkhand Massif, India. Applied Water Science. 8, 39.
DOI: https://doi.org/10.1007/s13201-018-0678-x

[47] Kelly, W.P., 1940. Permissible composition and concentration of irrigated waters. Proceedings of ASCF. 66, 607.

[48] Richards, L.A., 1954. Diagnosis and improvement of saline and alkali soils. Agricultural Handbook 60, U.S. Department of Agriculture, Washington, D.C. pp. 160.

[49] Doneen, L.D., 1964. Notes on water quality in Agriculture. Published as a Water Science and Engineering, Paper 4001, Department of Water Sciences and

Engineering, University of California.
[50] Ryznes, J.W., 1944. A new index for determining amount of calcium carbonate scale formed by water. Journal American Water Works Association. 36, 472-486.
[51] Kim, K., Yun, S., Choi, B., et al., 2009. Hydrochemical and multivariate statistical interpretations of spatial controls of nitrate concentrations in a shallow alluvial aquifer around oxbow lakes (Osong area, central Korea). Journal Of Contaminant Hydrology. 107, 114-127.
[52] Indian Standard Institute (ISI), 1974. Characteristics of inland surface water. IS, New Delhi, 2490.